View metadata, citation and similar papers at core.ac.uk

brought to you by CORE

provided by ScholarWorks@UNIST

Dielectric response of polymer films confined between mica surfaces

Yoon-Kyoung Cho, Hiroshi Watanabe, and Steve Granick

Citation: The Journal of Chemical Physics **110**, 9688 (1999); doi: 10.1063/1.478933

View online: http://dx.doi.org/10.1063/1.478933

View Table of Contents: http://scitation.aip.org/content/aip/journal/jcp/110/19?ver=pdfcov

Published by the AIP Publishing

Articles you may be interested in

Aging and stiction dynamics in confined films of a star polymer melt
J. Chem. Phys. **137**, 194702 (2012); 10.1063/1.4766468

Dielectric relaxation and alternating current conductivity of lanthanum, gadolinium, and erbium-polyvinyl alcohol doped films
J. Appl. Phys. **112**, 034102 (2012); 10.1063/1.4739752

Dielectric relaxation in polyimide nanofoamed films with low dielectric constant
Appl. Phys. Lett. **92**, 052910 (2008); 10.1063/1.2840715

Low-temperature dielectric properties of Langmuir–Blodgett ferroelectric polymer films
J. Appl. Phys. **103**, 034110 (2008); 10.1063/1.2838212

Dielectric properties of fluorocarbon thin films deposited by radio frequency sputtering of polytetrafluoroethylene
J. Appl. Phys. **92**, 4584 (2002); 10.1063/1.1505983

This article is copyrighted as indicated in the article. Reuse of AIP content is subject to the terms at: http://scitation.aip.org/termsconditions. Downloaded to IP: 114.70.7.203 On: Fri, 05 Sep 2014 08:26:15

Dielectric response of polymer films confined between mica surfaces

Yoon-Kyoung Cho
Department of Materials Science and Engineering, University of Illinois, Urbana, Illinois 61801

Hiroshi Watanabe
Institute for Chemical Research, Kyoto University, Uji, Kyoto 611, Japan

Steve Granick[a)]
Department of Materials Science and Engineering, University of Illinois, Urbana, Illinois 61801

(Received 21 December 1998; accepted 18 February 1999)

The thin-film dielectric response of organic films confined within a surface forces apparatus (SFA) and also between parallel sheets of atomically smooth mica is reported for the first time. Analysis is presented to infer dielectric properties of the organic film from the measured capacitance of the total system: sample, and mica sheets intervening between sample and electrodes. Measurements concerned the frequency dependence of normal-mode dielectric relaxation of *cis*-polyisoprene having dipoles aligned in the same direction along the chain backbone. We find that in thin-film geometries the peak frequency, f_{peak}, of normal mode dielectric loss (ϵ'') is moderately lower than for bulk samples and that, more important, the expected terminal tail, observed in the bulk sample ($\epsilon'' \propto f$ for $f < f_{\mathrm{peak}}$), is not observed even at the lowest frequency examined. Thus the slow normal mode distribution is much broader and the terminal relaxation time is much longer for chains in the thin layers. These dielectric features are attributed to spatial constraints on global chain motion in the thin layers and also to adsorption of chains on mica surfaces when the layer thickness is comparable to the unperturbed chain dimension. Independent measurements of shear relaxation, performed using a SFA modified for measurement of dynamical mechanical shear rheology, found a tremendously retarded viscoelastic response relative to bulk samples. There is the possibility that the broad distribution of the dielectric response of individual polymer chains may correspond to the observed retarded viscoelastic relaxation. However, we cannot rule out the other possibility that the dielectrically detected relaxation of individual chains is still faster than the terminal viscoelastic relaxation and that the latter thus corresponds to the collective motion of many confined chains.
© *1999 American Institute of Physics.* [S0021-9606(99)50419-4]

I. INTRODUCTION

There is no adequate experimental understanding of confined liquids (liquid films whose thickness approaches dimensions of the molecules themselves)—not in the sense that liquids in the bulk (isotropic) state have long been studied at length using many methods.[1] Part of the impediment to experimental progress can be traced to the paucity of experimental probes with sufficient sensitivity to probe molecularly thin films.

We are concerned here with fluids confined symmetrically between opposed flat surfaces. One motivation is that this geometry is particularly well defined relative to an alternative approach, to confine the fluid within a porous medium with fine pores.[2–4] A pore geometry contains intrinsic heterogeneity, both as concerns surface chemistry and as concerns surface curvature, that can be avoided when measurements involve flat surfaces. A second motivation is that this geometry affords the possibility to apply, during measurement, external fields such as shear, which cannot be applied in porous media. Still other prior related work on confined fluids concerns films confined on one side by solid and on the other side by air or vacuum.[5] We seek here to address the physical problem in which this asymmetry is absent.

The difficulty is to find an experiment with sufficient resolution—the quantity of the sample is small and the experimental probe must pass through a buried interface. This profound technical difficulty explains why most such measurements to date have been restricted to the measurement of mechanical forces. The surface forces apparatus has been employed widely for this purpose.[6] More recently, atomic force microscopy, friction force microscopy, and modifications of these techniques have also been employed. All such force measurements share the advantage of sensitivity but also the limitation that force is the collective, macroscopic response of a large collection of molecules. How to obtain information about confined fluids that is more intrinsically molecular in character?

We describe here what we believe to be the first successful application of dielectric spectroscopy to this purpose. Recent related research by others has investigated ultrathin Langmuir–Blodgett films confined between gold metal films,[7] but those studies suffered from surface roughness, from uncertainties regarding the effects of metal evaporation on the intervening organic film,[8] and from uncertain determination of the actual film thickness. In these prior dielectric

[a)]Author to whom all correspondence should be addressed.

 © 1999 American Institute of Physics

This article is copyrighted as indicated in the article. Reuse of AIP content is subject to the terms at: http://scitation.aip.org/termsconditions. Downloaded to IP: 114.70.7.203 On: Fri, 05 Sep 2014 08:26:15

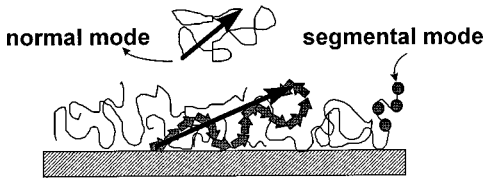

FIG. 1. Schematic diagram of flexible chains adsorbed from the melt to a solid surface. *Cis*-polyisoprene has dipoles parallel to the chain backbone and its slowest relaxation time therefore reflects the slowest normal modes of single molecules. It also has the component of dipole moment perpendicular to the chain and thus exhibits the segmental mode process as well, which is molecular-weight independent and appears at high frequencies not covered in the present experiments.

studies, discernible differences between bulk and thin-film properties were not observed.

II. EXPERIMENT

A. Materials choice and experimental procedures

A schematic diagram of this type of flexible polymer adsorbed from the melt to a solid surface is shown in Fig. 1. As the confined fluid, we selected polymer chains whose dipoles lie in the same direction parallel to the chain backbone and whose slowest relaxation time therefore reflected the slowest normal modes of single molecules. Since *cis*-polyisoprene also has the component of dipole moment perpendicular to the chain, it also exhibits the segmental mode process, which is molecular weight independent.

Cis-polyisoprene (PI) was selected for three reasons. First, anionically polymerized samples of narrow chain length distribution can be easily synthesized and even more easily purchased from commercial supply houses. Second, issues of adsorbed moisture and polar contamination, which can be troublesome in many dielectric measurements,[9] become a relatively minor issue because this polymer is so nonpolar. Third, block copolymers of polyisoprene with other polymers, polymers that can anchor the PI block to an interface, are also easily available, thus affording the possibility to study the dielectric responses of end-tethered polymer ''brushes.''

Cis-polyisoprene (PI) was purchased from Polymer Sources (Quebec) with number-average molecular weight $M_n = 6000$ and $14\,500\ \mathrm{g\,mol^{-1}}$ and ratio of weight-average to number-average molecular weight $M_w/M_n = 1.04$ for both of the samples. All data presented below were taken at room temperature, 25 °C.

Muscovite mica was cleaved in a laminar flow cabinet by traditional methods to give atomically smooth, step-free sheets of thickness 1–3 μm and area $\approx 1\ \mathrm{cm^2}$. For the experiments made within the surface forces apparatus, the polymer-laden surfaces were incubated in the presence of a hygroscopic chemical, P_2O_5, before bringing the mica surfaces close together, and subsequent measurements were also made in the presence of P_2O_5. This was not feasible for the experiments with spin-coated films (see Sec. III). In those cases the time spent exposed to the atmosphere, before forming the sandwich geometry described in Sec. III, was minimized to <10 min.

Dielectric data were acquired using a Solartron 1260 Gain-Phase Impedance Analyzer connected to a Solartron 1296 Dielectric Interface. All data were taken with the sample placed inside a sealed chamber, in the presence of P_2O_5 to keep the atmosphere dry.

In implementing these measurements, one challenge was to keep the applied voltage sufficiently small to prevent significant electric-field-induced attraction between the electrodes.[10] In the experiments described below, we found it possible to obtain a useful signal with only $0.1V_{\mathrm{rms}}$. The resulting attractive force between opposed mica surfaces was then only 5 nN for a typical mica film thickness of 3 μm. For measurements made in the surface forces apparatus (SFA) using our spring constant of $1000\ \mathrm{N\,m^{-1}}$, 5 nN force can induce only a 0.05 Å change of surface spacing even in the absence of repulsive forces that would impede this change. For the parallel-plate geometry described below, the voltage-induced deformation was even less.

Calibration of the empty cell response (see below) involved using the same mica sheets used in the subsequent measurements. The method was usually to cleave a large area of step-free mica and to divide this into four smaller sheets: two used for calibration, and two used for measurements. When squeezing the sample between mica in the SFA experiments, only two sheets were required, the calibration being performed before adding the sample.

B. Geometries and analysis used in dielectric measurements

The dielectrically examined PI layers were prepared on the mica sheets by several different methods: bulk squeezing, adsorption, and spin casting. The method chosen was intimately related to the geometry of dielectric measurement as explained below. To avoid some confusion, the sample preparation methods are explained only briefly in Sec. II B, and additional detail is given in Sec. III, just before presenting the dielectric data obtained in the respective geometries.

1. Experiments in the SFA

In the surface forces apparatus (SFA), film thickness is determined by multiple beam interferometry between silver films that have been coated onto the backsides of mica surfaces. In our experiments, we found it convenient to employ silver films 660 Å thick, deposited by vacuum sputtering. These continuous silver films were employed as electrodes for dielectric measurement of samples between the intervening mica plates.

The initial measurements were made between crossed mica cylinders within a surface forces apparatus itself. However, a fundamental difficulty in analyzing such measurements soon became apparent: Owing to the crossed-cylinder geometry, large portions of the dielectrically active sample were positioned at larger separations than the point of closest approach. This presented a severe problem since capacity scales only linearly with inverse film thickness. For the similar problem of hydrodynamic drainage forces between crossed cylindrical surfaces, which also scale as 1/(film thickness), a quantitative analysis has been presented previously.[11]

This article is copyrighted as indicated in the article. Reuse of AIP content is subject to the terms at: http://scitation.aip.org/termsconditions. Downloaded to IP: 114.70.7.203 On: Fri, 05 Sep 2014 08:26:15

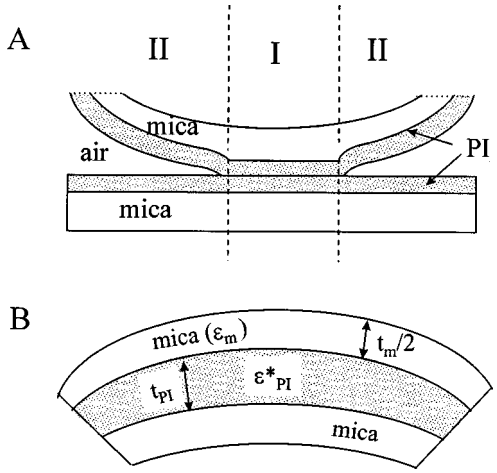

FIG. 2. Geometries for dielectric measurements of ultrathin fluid films. The top panel (A) illustrates the crossed-cylinder geometry of a surface forces apparatus (SFA), which is equivalent in projection to a sphere-on-flat geometry. The mica sheets bearing thin adsorbed polymers layers (hatched regions) come into contact where the spherical curvature meets the flat opposing surface (zone I) and elsewhere are separated by air or gas (zone II). The bottom panel (B) illustrates the parallel-plate geometry produced by containing a thin polymer film of thickness t_{PI} between two sheets of mica of uniform thickness $t_m/2$ for each mica sheet. The drawing is not to scale and in practice, $t_{PI} \ll t_m$. The backside of each mica sheet is coated by a silver electrode to which oscillatory voltage is applied. The resulting frequency-dependent capacitance is the serial result of the dielectric constant of mica (ϵ_m) and polyisoprene sample (ϵ^*_{PI}).

Seeking to minimize this difficulty, we draped the mica sheets over crossed cylinders whose radius of curvature was two orders of magnitude larger than in the traditional surface forces apparatus—radius of curvature 0.5 m rather than the typical 2 cm—but came to appreciate that this presented no fundamental solution.

We next took the strategy to allow the polymer to adsorb onto mica from dilute solution, then to dry the layers, and finally to bring the dried layers into opposed contact. The advantage of this protocol was to eliminate the possibility of dielectric response from the polymer at thickness larger than that of the opposed dry polymer layers. The geometry is illustrated in Fig. 2(A). There was a zone of closest approach (flat contact) between crossed cylinders [zone I in Fig. 2(A)] and a zone of larger separation (zone II). We neglect an effect of surface curvature in zone II to make the following dielectric analysis. For this situation, the dielectric setup shown in Fig. 2(A), the complex capacity C^*_I for region I is given as

$$\frac{1}{C^*_I} = \frac{1}{C_{mI}} + \frac{1}{C^*_{PI}} = \frac{1}{C_{mI}} + \frac{1}{\epsilon^*_{PI} C_{I0}}, \tag{1}$$

where C_{mI} is the capacitance of the two mica layers in zone I (mica is considered to have no dielectric loss and C_{mI} is a real number), C_{I0} is the vacant capacitance for the hatched zone in zone I, and ϵ^*_{PI} is the complex dielectric constant for the thin (confined) PI layer in this zone.

Since the mica layer is much thicker than the PI layer ($C_{mI} \ll C_{I0}$), Eq. (1) becomes

$$C^*_I \cong C_{mI}\left[1 - \frac{C_{mI}}{\epsilon^*_{PI} C_{I0}}\right]. \tag{2}$$

Similarly, the dynamic capacity for zone II is

$$C^*_{II} \cong C_{mII+air}\left[1 - \frac{C_{mII+air}}{\epsilon^*_{PI} C_{II0}}\right] \quad (C_{mII+air} \ll C_{II0}), \tag{3}$$

where $C_{mII+air}$ is the capacitance of the two mica layers plus air gap in zone II (and $C_{mII+air}$ is assumed to be a real number), and C_{II0} is the vacant capacitance for the hatched region in zone II. Here, the PI layer is *assumed* to have the same dielectric constant in zones I and II.

From Eqs. (2) and (3), the complex capacity of the whole system is

$$C^*(\omega) = C^*_I + C^*_{II} = C_{bare} - \frac{Q}{\epsilon^*_{PI}}, \tag{4}$$

where ω denotes angular frequency and $C_{bare} = [C_{mI} + C_{mII+air}]$ is the capacity of the two mica sheets that are brought into bare contact (in air) keeping their surface profile identical to that in Fig. 2(A) (i.e., identical to that in the case of sustaining the adsorbed PI layer), and Q is defined as

$$Q = \left[\frac{C^2_{mI}}{C_{I0}} + \frac{C^2_{mII+air}}{C_{II0}}\right]. \tag{5}$$

In principle, one may use Eq. (4) to evaluate ϵ^*_{PI} from the measured C^*. However, the quantities necessary for this evaluation, C_{bare} and Q, are hard to estimate or to determine from independent experiments. In addition, since the adhesion and the applied load will not be the same for bare mica contact and mica in the presence of an intervening film, the surface profile of the mica sheets in the presence of a thin polymer layer is expected to differ from that measured during a calibration of the capacity during mica–mica contact. Therefore no simple feasible experimental method is evident to determine C_{bare} from a calibration experiment in the absence of polymer. On the other hand, calculation of C_{bare} is disturbed by complex curvature in a crossed cylindrical geometry. Similarly, the calculation of Q includes a huge uncertainty. Because of the above difficulties, we did not attempt to evaluate the magnitude of ϵ^*_{PI} for measurements made in this geometry. Instead, we examined only the frequency dependence of ϵ^*_{PI}, which represents the relative distribution of dielectric modes.

For this purpose, we express $\epsilon'_{PI}(\omega)$ as $\epsilon'_{PI}(\omega) = \epsilon_{\infty,s} + \epsilon'_n(\omega)$. Here, $\epsilon_{\infty,s}$ is the dielectric constant at high ω where the normal mode relaxation has not (significantly) occurred; $\epsilon_{\infty,s}$ is due to segmental motion and very fast atomic/electronic polarization. The quantity $\epsilon'_n(\omega)$ is the relaxing part of $\epsilon'(\omega)$ due to the global motion of the PI chain (i.e., ϵ' for the normal mode relaxation); $\epsilon'_n(\infty) = 0$ and $\epsilon'_n(0) = \Delta\epsilon_n$ (the dielectric intensity of the normal mode relaxation). At time scales of the normal mode relaxation, the measured $\epsilon''_{PI}(\omega)$ of the whole system coincides with the loss $\epsilon''_n(\omega)$ due to the normal modes.

For bulk PI melts, $\Delta\epsilon_n/\epsilon_{\infty,s} \cong 0.05$ and $\epsilon''_n(\omega)/\epsilon_{\infty,s} < 0.02$. These ratios should be even smaller for the thin adsorbed PI layer. (As explained below, $\Delta\epsilon_n$ decreases on the

This article is copyrighted as indicated in the article. Reuse of AIP content is subject to the terms at: http://scitation.aip.org/termsconditions. Downloaded to IP: 114.70.7.203 On: Fri, 05 Sep 2014 08:26:15

decrease of the PI chain dimension, r_e, measured in the direction of the applied field.) Considering this point for $C^*=C'-iC''$ given in Eq. (4), we can write C'' as

$$C^*(\omega)=Q\frac{\epsilon^*_{\rm PI}(\omega)}{\{\epsilon'_{\rm PI}(\omega)\}^2+\{\epsilon'_{\rm PI}(\omega)\}^2}\cong\left[\frac{Q}{\{\epsilon_{\infty,s}\}^2}\right]\epsilon^*_n(\omega). \qquad (6)$$

Thus, the measured C'' has the ω dependence identical to that of ϵ''_n, meaning that the normal mode distribution can be examined for $C''(\omega)/C''_{\rm peak}=\epsilon''_n/\epsilon''_{n,\rm peak}$, i.e., by reducing both to these respective peak values.

A related point is to note that the static dielectric constant is given by the expression $\epsilon'_{\rm PI}(0)=\epsilon_{\infty,s}+\Delta\epsilon_n$. On physical grounds, we expect $\epsilon_{\infty,s}$ to be more likely the same for the cases of bulk and thin films; but it is natural to expect that $\Delta\epsilon_n$ may differ for thin layers owing to expected perturbations of the random coil configuration (discussed further below). By this reasoning, it would be incorrect to support the notion that $\epsilon'_{\rm PI}(0)$ is the same for the bulk system and the thin films.

2. Parallel sheets of mica

For improved definition of the experimental geometry, it was desirable to produce a uniform film thickness everywhere in the sample—to avoid the crossed cylinder geometry that is intrinsic to a surface forces apparatus. To this end, we employed spin-coating, as described experimentally in Sec. III. The experimental geometry is sketched in Fig. 2(B). The resulting intimate contact between sample and both mica sheets was corroborated by interferometric measurements. The film thickness and surface contour were measured by multiple beam interferometry between silver films on the backsides of the mica, using the same optical setup as for the surface forces apparatus, and using solid supports with 2 cm radius of curvature. The constant fringe–fringe spacing, regardless of spatial position over the large lateral dimension of hundreds of micrometers, showed the excellent extent to which the surface–surface spacing was the same throughout.

For the dielectric setup shown in Fig. 2(B), the complex capacity C^* is given as

$$C^*=\left[\frac{1}{C_m}+\frac{1}{\epsilon^*_{\rm PI}C_{\rm I0}}\right]^{-1}$$

$$=C_m\left[1+\frac{t_{\rm PI}\epsilon_m}{t_m\epsilon^*_{\rm PI}}\right]^{-1}\cong C_m\left[1-\frac{t_{\rm PI}\epsilon_m}{t_m\epsilon^*_{\rm PI}}\right]\quad(t_{\rm PI}\ll t_m), \qquad (7)$$

where C_m is the capacitance of the two mica layers, t_m is the total thickness of the two mica layers, ϵ_m is the (ω-insensitive) dielectric constant of mica, and $t_{\rm PI}$ is the thickness of the thin, spin-coated PI layer. For this setup, C_m is identical to the capacity measured for the bare mica–mica contact, and t_m and $t_{\rm PI}$ are known from optical interferometry. The quantity ϵ_m can be calculated from C_m (if the electrode area is known), or can be replaced by a literature value. Thus in principle it is possible to evaluate $\epsilon^*_{\rm PI}$ from experimentally measured values, but the method requires accurate calibration of the empty cell (bare mica capacitance), as discussed in Sec. III.

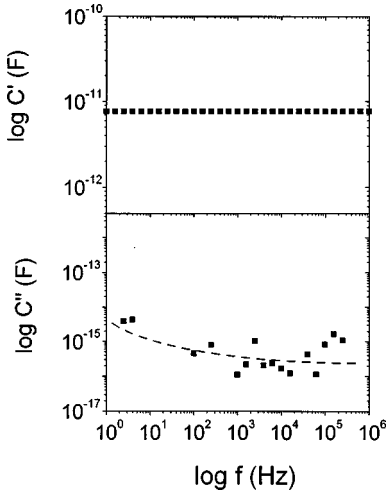

FIG. 3. Illustration of the capacitance measured within a surface forces apparatus (SFA) for mica–mica contact in dry air atmosphere. Capacitance in phase with the externally applied electric field (C') and capacitance 90° out of phase with the externally applied electric field (C'') are plotted on log–log scales against the frequency of the applied electric field. One sees that C' is frequency independent and that C'' is negligibly small, $C''/C'\approx 10^{-4}$.

III. RESULTS AND DISCUSSION

The measurements were performed at the University of Illinois. First, as a point of reference, Fig. 3 shows dielectric measurements when two sheets of mica were brought together in dry atmosphere within the surface forces apparatus. The top panel shows the in-phase capacitance, $C'(f)$, plotted against the logarithmic Hertzian frequency, f. The bottom panel shows the component 90° out of phase, $C''(f)$. (It is conventional, in representing dielectric data, to plot f rather than the angular frequency, ω). C' exhibits no frequency dependence, and the magnitude of dielectric loss was negligible, on the order of 10^{-4} times the in-phase component, justifying the assumptions made in Sec. II. Complications when measurements were not performed in dry atmosphere are discussed below.

The data in Fig. 3 illustrate the experimental sensitivity required. For a frustrating period of time when our experiments began, stray capacitance in the device exceeded the magnitude of the interesting signal. It was necessary to pay excruciating attention to fine details of electrical connections, the length of wires, and the geometrical arrangement of various metal parts in the vicinity of the sample.

A. Comparison of dielectric data in thin film and bulk systems

1. Experiments in the SFA

As explained in Sec. II B, for experiments within the surface forces apparatus it was problematical to distinguish the dielectric response of the bulk fluid from that of the fluid at the point of closest approach between the crossed cylinders. Seeking to circumvent this difficulty, we took the strategy to allow PI to adsorb onto mica from dilute cyclohexane solution (10 mg $\rm mL^{-1}$), then to dry the adsorbed layers under a flow of argon (12 h), and finally to bring the dried layers into opposed contact within the SFA. The measured thick-

This article is copyrighted as indicated in the article. Reuse of AIP content is subject to the terms at: http://scitation.aip.org/termsconditions. Downloaded to IP: 114.70.7.203 On: Fri, 05 Sep 2014 08:26:15

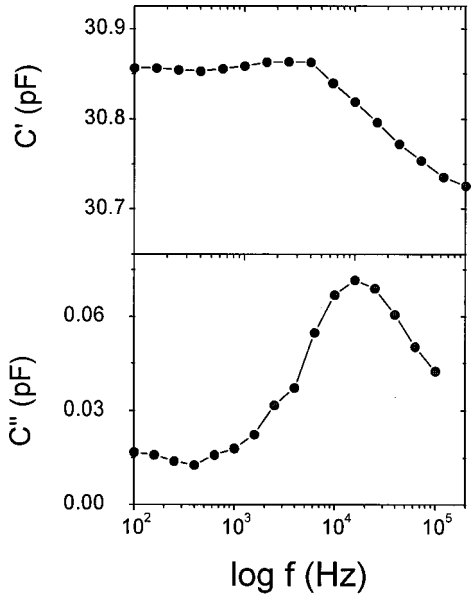

FIG. 4. Capacitance measured in the surface forces apparatus for crossed cylinders of mica coated with dried adsorbed layers of *cis*-polyisoprene (PI) as described in the text. Thickness at the closest approach of these PI films ($M_n = 6000\ \mathrm{g\ mol^{-1}}$) was 30 Å. The top panel shows the in-phase capacitance, C', and the bottom panel shows the out-of-phase capacitance, C''. Both are plotted against the Hertzian frequency of the externally applied electric field.

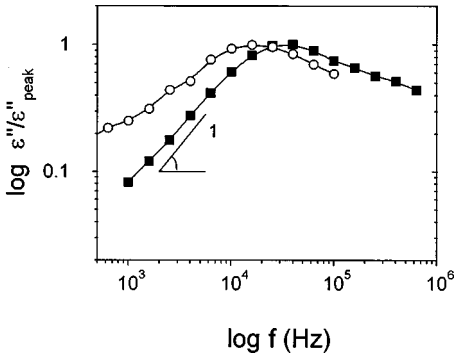

FIG. 5. Comparison of the dielectric mode distribution of a bulk and thin-film sample, both measured in a surface forces apparatus (SFA). The out-of-phase dielectric constant of PI ($M_n = 6000\ \mathrm{g\ mol^{-1}}$), obtained from Eq. (6) by normalizing $\epsilon''(f)$ by the intensity of response at the peak frequency, $\epsilon''_{\mathrm{peak}}$, is plotted on log–log scales against frequency, *f*. Closed squares refer to a polymer droplet of macroscopic thickness. Open circles refer to adsorbed PI layers placed into opposed contact (data taken from Fig. 4). Expected terminal behavior is observed for the bulk sample ($\epsilon'' \propto f$ below $\epsilon''_{\mathrm{peak}}$) but the *f* dependence is weaker for the thin-film samples even at the lowest frequency examined.

ness of the opposed dry PI layers in argon was 30 Å; by experimental design, the experiment contained no bulk fluid.

Measurements of the resulting dielectric response are shown in Fig. 4. The top panel of Fig. 4 shows the in-phase capacitance, $C'(f)$ and the bottom panel shows the component 90° out of phase; both components are plotted against the frequency of applied electric field, *f*. As must be expected on physical grounds, the former was independent of frequency until the advent of significant dielectric loss and the subsequent peak in $C''(f)$ was accompanied by a decrease of $C'(f)$.

Comparison to the dielectric response of this same bulk sample (i.e., a sample of macroscopic thickness) is shown in Fig. 5. Using the analysis described in Sec. II B, the ratio of loss dielectric response relative to that of the peak intensity, $\epsilon''/\epsilon''_{\mathrm{peak}}$, is plotted on log–log scales against frequency of the applied electric field normal to the thin film. Filled squares are the normalized loss data obtained in the SFA with a macroscopic gap width t_g. (This is still much smaller than the surface curvature so that we could safely neglect the effect of curvature on the dielectric signal. For this case, ϵ''_{PI} was determined as $C''(\omega)/C_0$, with C_0 being the capacity of the vacant cell having the width of t_g). The ϵ''_{PI} data of bulk PI determined in this way agree with literature data[12] obtained with a conventional dielectric cell.

Note that the peak frequency of ϵ''_{PI} is lower for the adsorbed layer than for the bulk PI by a factor ≈ 2; the peak frequency shifted from 35 to 15 kHz. More importantly, the bulk PI system exhibited the terminal tail ($\epsilon'' \propto f$) soon after *f* decreased from f_{peak} while the tail was not observed for the adsorbed layer even for the lowest *f* examined.

Thus the slow normal mode distribution was much broader and the terminal relaxation time much longer for the PI chains in the thin layer. But for films so thin, it was not possible to separate the respective influences of spatial confinement within a thin layer from constraint on chain motion owing to adsorption of segments to the solid surfaces.

2. Experiments made in parallel geometry

To form a thin polymer film in parallel geometry, the polymer sample was first dissolved in cyclohexane to a concentration from 1 to 25 $\mathrm{mg\ mL^{-1}}$ depending on the desired film thickness, spin-coated onto a freshly cleaved sheet of atomically smooth mica, and finally a sheet of cleaved mica of this same thickness was placed on top. Capillary forces pulled the second sheet onto the underlying polymer sample, thus forming a sandwich geometry. The resulting surface spacing was measured by multiple beam interferometry between silver electrodes on the backsides of the mica and parallel alignment was verified.

However in our current experimental setup it was not possible to perform these experiments in an atmosphere sufficiently dry to obtain a sufficiently reliable evaluation of C_m (mica–mica contact). The influence of moisture condensed on the mica surfaces became plain when measurements were performed in nominal mica–mica contact (two cleaved mica sheets placed in contact). The ratio C''/C' was $\approx 10^{-4}$ for measurements made within the SFA, $\approx 10^{-3}$ for measurements made immediately after drying cleaved mica sheets in a vacuum oven at 150 °C for 2 h, and in one instance $\approx 10^{-2}$ (even higher at the lowest f) when made without precautions made to dry the mica before measurement. There then resulted a large uncertainty in the capacitance of the two mica layers, C_m, and it was not possible to be confident that C_m measured for mica–mica contact remained the same after spin-coating with PI. Attempts to apply Eq. (7) to evaluate ϵ^*_{PI} gave the nominal result that ϵ' took a value less than unity, which is physically unrealistic.

This article is copyrighted as indicated in the article. Reuse of AIP content is subject to the terms at: http://scitation.aip.org/termsconditions. Downloaded to IP: 114.70.7.203 On: Fri, 05 Sep 2014 08:26:15

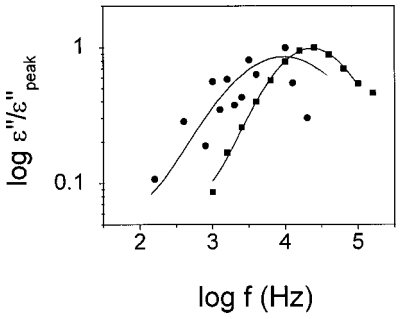

FIG. 6. Comparison of the dielectric mode distribution of a bulk and thin-film sample, both measured in the parallel-plate geometry indicated in Fig. 2(B). The out-of-phase dielectric constant of PI ($M_n = 6000\ \mathrm{g\,mol^{-1}}$, $M_w/M_n = 1.04$), obtained from Eq. (6) by normalizing $\epsilon''(f)$ by the intensity of response at the peak frequency, ϵ_{peak} is plotted against logarithmic frequency, *f*. The data concern a sample of macroscopic thickness (squares) and PI thin film of thickness 64 Å (circles). The solid lines are presented as guides to the eyes.

For measurements made in parallel-plate geometry, the out-of-phase dielectric constant of PI ($M_n = 6000\ \mathrm{g\,mol^{-1}}$), obtained from Eq. (6) by normalizing measured C'' data by the intensity of response at the peak, is plotted in Fig. 6 on log–log scales against the logarithmic frequency of the externally applied electric field for a droplet of macroscopic thickness (squares) and PI film of thickness 64 Å (circles).

But in general, such normalization was not feasible. Difficulties in evaluating C_m, which is needed in order to apply Eq. (7), led us to provisionally adopt a different approach to compare between measurements made under various conditions. Normalized dielectric spectra were defined as:

$$\epsilon_r'(f) \equiv 2.3C'(f)/C(100\ \mathrm{Hz}), \tag{8}$$

$$\epsilon_r''(f) \equiv 2.3C''(f)/C(100\ \mathrm{Hz}), \tag{9}$$

where *f* denotes the frequency of the applied electric field, *C* denotes the absolute magnitude of capacitance, and the number 2.3 is the zero-frequency dielectric constant of *cis*-polyisoprene, which we assume in this normalization to be unaffected at zero frequency by the film thickness. The frequency 100 Hz, a frequency at which $C'(f)$ was essentially frequency independent in these experiments, was selected for convenience. While it is true that general arguments presented in Sec. II B 1 lead one to expect $C'(0)$ to differ between bulk samples and this same material in a thin film (which means that it will be necessary, in future work, to develop better ways to calibrate C_m), for the present experiments at relatively large film thickness, relative to experiments described here for the SFA geometry, this method of normalization was used provisionally.

Dielectric measurements made in this sandwich geometry are presented in Fig. 7. The normalized dielectric response of PI in phase with the electric field (the top panel) and 90° out of phase (the bottom panel) are plotted against logarithmic frequency of the applied electric field. One observes that the intensity of the dielectric peak associated with normal mode relaxation decreased tremendously with decreasing film thickness. In addition, this peak broadened in breadth and grew, with increasing value of the applied frequency *f*, less and less strongly than directly proportional to

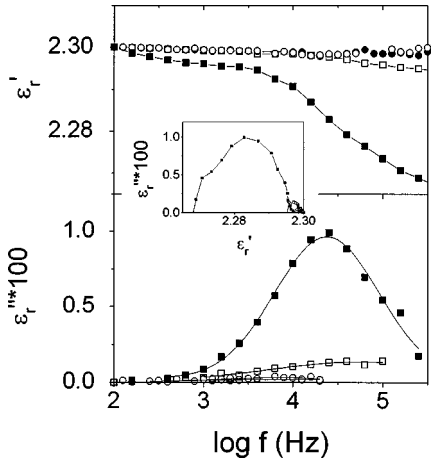

FIG. 7. Comparison of measurements made in parallel-plate geometry concerning spin-coated films of *cis*-polyisoprene ($M_n = 6000\ \mathrm{g\,mol^{-1}}$, $M_w/M_n = 1.04$) confined between atomically smooth muscovite mica. The normalized responses in phase with the electric field [$\epsilon_r'(f)$, the top panel] and 90° out of phase [$\epsilon_r''(f)$, the bottom panel], are plotted against Hertzian frequency, *f*, after normalization using Eqs. (8) and (9). The data concern films of macroscopic thickness (closed squares), 572 Å thickness (open squares), 285 Å thickness (closed circles), and 64 Å thickness (open circles). Thickness was determined by multiple beam interferometry. The inset shows $\epsilon_r''(f)$ plotted against $\epsilon_r'(f)$, i.e., a Cole–Cole plot.

f as the film thickness decreased. It is as if the intensity of response shifted to a broader frequency range, even passing to frequencies lower than could be observed over the instrument's span of frequency measurement.

Similar data obtained with a PI sample of different molecular weight ($M_n = 14\,500\ \mathrm{g\,mol^{-1}}$) are presented in Fig. 8, with similar conclusions. Thus—in qualitative agreement with measurements made in the SFA, but in these cases con-

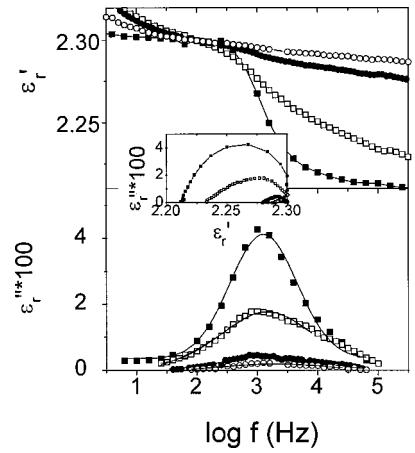

FIG. 8. Comparison of measurements made in parallel-plate geometry concerning spin-coated films of *cis*-polyisoprene ($M_n = 14\,500\ \mathrm{g\,mol^{-1}}$, $M_w/M_n = 1.04$) confined between atomically smooth muscovite mica. The normalized response in phase with the electric field [$\epsilon_r'(f)$, the top panel] and 90° out of phase [$\epsilon_r''(f)$, the bottom panel], are plotted against Hertzian frequency, *f*, after normalization using Eqs. (8) and (9). The data concern films of macroscopic thickness (closed squares), 1075 Å thickness (open squares), 740 Å thickness (closed circles), and 285 Å thickness (open circles). Thickness was determined by multiple beam interferometry. The inset shows $\epsilon_r''(f)$ plotted against $\epsilon_r'(f)$, i.e., a Cole–Cole plot.

This article is copyrighted as indicated in the article. Reuse of AIP content is subject to the terms at: http://scitation.aip.org/termsconditions. Downloaded to IP: 114.70.7.203 On: Fri, 05 Sep 2014 08:26:15

cerning films whose film thickness was uniform—these thin-film samples displayed broad normal-mode distribution and retardation of the terminal relaxation.

A dielectric measurement quantifies fluctuation of the polarization in the direction perpendicular to the electrode surfaces. For a chain in a bulk isotropic medium, the dielectric relaxation strength for the normal mode is proportional to $\langle r_e^2 \rangle$, the mean square end-to-end distance between chain ends. In a thin film, $\langle r_e^2 \rangle$ may in principle be smaller. In the limiting case of the thinnest films, it certainly cannot exceed the square of the gap width.

To quantify this effect, we remember that the dielectric intensity of the normal modes, $\Delta\epsilon_n = \epsilon'_{\mathrm{PI}}(0) - \epsilon_{\infty,s} = (2/\pi)\int_{-\infty}^{\infty} \epsilon_n^*(\omega) d \ln \omega$, is proportional to the square of the PI chain dimension ($\langle r_e^2 \rangle$) measured in the direction of the electric field *if* the chain can eventually lose its memory of the initial conformation and relax completely. If the chain cannot completely relax and loses only a fraction ϕ of its memory, $\Delta\epsilon_n$ is proportional to $\phi\langle r_e^2 \rangle$. The PI chains in the adsorbed layers (previous section) did not completely relax in the frequency range examined (i.e., lacked terminal zone relaxation) and their $\Delta\epsilon_n$ cannot be accurately determined from the available data.

However, the apparent intensity $\Delta\epsilon_{n,\mathrm{app}}$ of the better defined sandwiched geometry, estimated from the Cole–Cole plots (inserts in Figs. 7 and 8) was significantly decreased from the bulk $\Delta\epsilon_n$ value ($\cong$0.07–0.08) as the layer thickness was decreased below 572 Å (Fig. 7) and 740 Å (Fig. 8), even though the layer thickness still exceeded the unperturbed $\langle r_e^2 \rangle$ by an order of magnitude. This result might suggest that a fraction of initial memory is very long-lived and thus that only a fractional relaxation (this fraction being much less than unity) was reflected in $\Delta\epsilon_{n,\mathrm{app}}$ over the accessible frequency. For very thin layers having a thickness t less than the equilibrium end-to-end chain separation, $\langle r_e^2 \rangle$, the low value of t should also contribute to the decrease of $\Delta\epsilon_{n,\mathrm{app}}$. This might be the case for the layer with $t = 64$ Å (Fig. 7), but probably not for the layers of larger thickness.

Further studies are under way to compare the current preliminary data with that obtained using samples of higher molecular weight.

B. Comparison of dielectric and rheological data for thin layers

One of the main motives for this study is that extensive rheological and tribological experiments in recent years have found dynamical anomalies in ultrathin fluid films. These anomalies have in common the feature that rheological relaxation times are enormously prolonged relative to responses of these same systems in the bulk state. Therefore force measurements were performed on these same PI systems for comparison. The data in Fig. 9 show an effect of confinement on the static force-distance profile as the layer thickness was decreased below $5\langle r_e^2 \rangle^{1/2}$ (r_e referring, as in Sec. III A, to the equilibrium end-to-end distance). The effect of film thickness on the dynamic rheological moduli

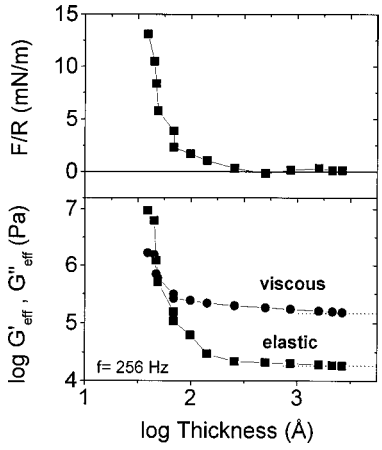

FIG. 9. Surface forces and shear viscoelastic properties measured for a droplet of *cis*-polyisoprene ($M_n = 6000\ \mathrm{g\ mol^{-1}}$, $M_w/M_n = 1.04$) confined between atomically smooth muscovite mica with radius of curvature $\approx$2 cm. (Top panel): Static force required to compress to a given surface separation, normalized by a mean radius of curvature of the cylindrical surfaces (F/R), plotted against film thickness. Films were equilibrated for 5–10 min at each datum. (Bottom panel): The effective shear moduli in phase and out of phase with the driving force, G'_{eff} (elastic) and G''_{eff} (viscous), plotted on log–log scales against film thickness for the same films shown in Fig. 2(A). The drive frequency was 256 Hz and the measurements were made in the linear-response regime (strain less than 5% of film thickness). Predominantly viscous responses, at the larger separations, switched to predominantly elastic responses when the film thickness was small, indicating tremendous retardation of the viscoelastic response. Note that viscoelastic anomalies were observed at much larger film thickness than the anomalies of static force and that the distance scale is logarithmic.

emerged at even larger thickness, starting at $\approx$1000 Å. It is worth emphasizing that the distance scale in Fig. 9 (the abscissa) is logarithmic.

To perform these experiments, a droplet of *cis*-polyisoprene was placed between freshly cleaved sheets of muscovite mica within a homebuilt surface forces apparatus.[13] The top panel of Fig. 9 shows the force required to compress the droplet to a given thickness; the data concern the sample with $M_n = 6000\ \mathrm{g\ mol^{-1}}$. The equilibration time was 5–10 min/datum. One observes that the film supported a measurable normal force beginning at rather large separations, $\approx$300 Å, which is to be compared with the estimated radius of gyration $R_G \approx 26$ Å.[14] The reasons for finding metastable surface forces at distances so large relative to a segmental length have been much discussed and are commonly attributed to the strong adsorption of an adsorbed polymer layer.[15] The bottom panel of Fig. 9 compares the accompanying resistance to sinusoidal shear deformation. The drive frequency was 256 Hz and the amplitude of deformation was $<$5%, small enough to produce a linear viscoelastic response. After decomposing the viscoelastic response into one component in phase with the drive and a second component 90° out of phase with it, in the manner described elsewhere,[16,17] the data were normalized for film thickness and deformation amplitude and expressed as effective elastic and viscous shear moduli, G'_{eff} and G''_{eff}, respectively. One observes that the effective shear moduli grew monotonically with diminishing film thickness and that at very small thickness, relaxation was so strongly retarded that G'_{eff} and G''_{eff} were reversed in their relative intensity.

This article is copyrighted as indicated in the article. Reuse of AIP content is subject to the terms at: http://scitation.aip.org/termsconditions. Downloaded to IP: 114.70.7.203 On: Fri, 05 Sep 2014 08:26:15

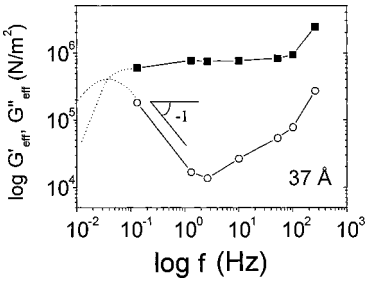

FIG. 10. Viscoelastic responses for the same polymer sample as in Fig. 9 confined to thickness 37 Å, which is close to the thickness for which dielectric measurements were made shown in Figs. 4 and 5. Effective shear moduli measured, G'_{eff} (elastic) and G''_{eff} (viscous), are plotted against frequency on log–log scales. From the extrapolated crossover frequency of viscous and elastic moduli (dotted lines), the mechanical relaxation frequency is estimated to be about 0.03 Hz. This should be compared with the slow normal mode distribution shown in Figs. 4 and 5.

To further quantify the strongly retarded viscoelastic relaxation observed for the thinnest films, the frequency dependence of the shear response was measured for a confined film of thickness 37 Å. In Fig. 10, G'_{eff} and G''_{eff} are plotted against shear frequency on log–log scales. It is evident that G''_{eff} shows a pronounced minimum, indicating a split of the viscoelastic shear response into two families of relaxation, at relatively low and at relatively high frequency. In the present paper, we are mainly concerned with relaxations at low frequency. Although the frequency range of measurements was limited to the data shown in Fig. 10, by extrapolating to the point where G'_{eff} and G''_{eff} cross we estimate the slowest shear relaxation frequency to be about 0.03 Hz.

Though the data in Figs. 9 and 10 were obtained in a squeezed droplet geometry, i.e., the geometry shown in Fig. 2(A) with the air gap filled with PI, the terminal relaxation in the squeezed droplet should be dominated by responses of PI chains in the thin confined layer [region I in Fig. 2(A)]. Thus we may compare the viscoelastic data (Figs. 9 and 10) with the dielectric data of the confined PI layer, the latter detecting decay of orientational memory (autocorrelation) of individual PI chains. Since the terminal dielectric relaxation of the thin layers is attained at $f<10^{2.5}$ Hz there is a possibility that the tremendously retarded terminal motion of individual PI chains could explain the viscoelastic relaxation shown in Figs. 9 and 10. To find large film thickness at the onset of perturbed chain relaxation is consistent with the perturbed dielectric relaxation presented in Figs. 7 and 8. However, it is tantalizing that the frequency of the peak of the dielectric loss for the thinnest films exceeded by so much the peak of mechanical loss. This suggests the interesting possibility that the rheological measurements at low frequency either were dominated by a subpopulation of confined chains, or reflected slow collective motions. Possible origins of collective motions have been discussed elsewhere.[18]

IV. CONCLUSIONS

In summary, dielectric measurements within a surface forces apparatus have been carried out; this is the first success so far reported. The setup of Fig. 2(A) is convenient to apply within a surface forces apparatus (SFA) and allows the examination of the dielectric mode distribution such as PI used in the present study, and also affords the possibility of performing measurements in the presence of other external fields such as shear. The setup of Fig. 2(B), though a little more difficult to implement, allows the examination of both distribution and absolute magnitude of the normal modes. Both types of measurement were performed in the course of this study and for both setups, significantly retarded dielectric relaxation was observed for thin polyisoprene (PI) layers, demonstrating the retardation of global chain motion owing to the combined effects of spatial confinement and surface adsorption. The measurements made between parallel sheets of mica concerned thicker films, where the layer thickness was larger than the unperturbed end-to-end distance of the polymer chain by an order of magnitude and adhesion should not represent a significant portion of the response.

In future studies, measurements at variable temperatures will be particularly informative, especially to compare loss peaks associated with normal mode relaxation with possible confinement-induced shifts of the segmental relaxation times. (At room temperature, these appeared at frequencies higher than our apparatus was able to measure.) Studies in these directions are in progress.

A key finding is that terminal behavior (loss proportional to frequency) was not observed in the thin films, even at the lowest frequencies that we could study. Whereas the peak of dielectric response observed in bulk samples is clearly assignable to fluctuation of the chain conformation (the slowest normal mode), the absence of terminal behavior in thin samples means that we cannot presently interpret the physical meaning of the peak frequency that we observed for the thin films, since it does not reflect a single relaxation process.

It remains intriguing that the measurements described in this paper show that the peak of dielectrically detected retarded relaxation of individual chains was still faster than the terminal viscoelastic relaxation. There is a possibility that the broad distribution of the dielectric response of individual polymer chains may correspond to the observed retarded viscoelastic relaxation. However, we cannot rule out the other possibility that the dielectrically detected relaxation of individual chains is still faster than the terminal viscoelastic relaxation and that the latter thus corresponds to collective motion of many confined chains. Examination of dielectric relaxation over wider ranges of frequency and temperature will resolve this problem.

ACKNOWLEDGMENTS

This material is based upon work supported by donors of the Petroleum Research Fund, administered by the American Chemical Society, and by the U.S. Department of Energy, Division of Materials Science under Award No. DEFG02-ER9645439, through the Frederick Seitz Materials Research Laboratory at the University of Illinois at Urbana–Champaign.

[1] P. A. Egelstaff, *An Introduction to the Liquid State*, 2nd ed. (Clarendon, Oxford, 1992).

This article is copyrighted as indicated in the article. Reuse of AIP content is subject to the terms at: http://scitation.aip.org/termsconditions. Downloaded to IP: 114.70.7.203 On: Fri, 05 Sep 2014 08:26:15

[2] M. Arndt, R. Stannarius, H. Groothues, E. Hempel, and F. Kremer, Phys. Rev. Lett. **79**, 2077 (1997).
[3] G. Barut, P. Pissis, R. Pelster, and G. Nimtz, Phys. Rev. Lett. **80**, 3543 (1998).
[4] Ch. Cramer, Th. Cramer, F. Kremer, and R. Stannarius, J. Chem. Phys. **106**, 3730 (1997).
[5] J. A. Forrest, K. Dalnoki-Veress, J. R. Stevens, and J. R. Dutcher, Phys. Rev. Lett. **77**, 2002 (1996).
[6] See, e.g., (a) S. Granick, Science **253**, 1374 (1991); (b) B. Bhushan, J. N. Israelachvili, and U. Landman, Nature (London) **374**, 607 (1995).
[7] A. Schmidt *et al.*, Macromolecules **28**, 5487 (1995).
[8] F. Kremer, *Dielectrics Newsletter* (Solartron Corp., April 1998).
[9] K. Adachi and T. Kotaka, Macromolecules **17**, 120 (1984); Prog. Polym. Sci. **18**, 585 (1993).
[10] P. Frantz, N. Agrait, and M. Salmeron, Langmuir **12**, 3289 (1996).
[11] J. Van Alsten, S. Granick, and J. N. Israelachvili, J. Colloid Interface Sci. **125**, 739 (1988).
[12] K. Adachi, and T. Kotaka, Macromolecules **18**, 466 (1985).
[13] J. Peachey, J. Van Alsten, and S. Granick, Rev. Sci. Instrum. **62**, 463 (1991).
[14] J. Bandrup and E. Immergut, *Polymer Handbook*, 3rd ed. (Wiley, New York, 1989).
[15] H.-W. Hu, S. Granick, and K. S. Schweizer, J. Non-Cryst. Solids **172-174**, 721 (1994).
[16] H.-W. Hu and S. Granick, Science **258**, 1339 (1992).
[17] S. Granick and H.-W. Hu, Langmuir **10**, 3857 (1994).
[18] G. Adam and J. H. Gibbs, J. Chem. Phys. **43**, 139 (1965).

This article is copyrighted as indicated in the article. Reuse of AIP content is subject to the terms at: http://scitation.aip.org/termsconditions. Downloaded to IP: 114.70.7.203 On: Fri, 05 Sep 2014 08:26:15